

Initial demonstration of AlGaAs-GaAsP- β -Ga₂O₃ n-p-n double heterojunctions

Jie Zhou¹, Ashok Dheenan², Jiarui Gong¹, Carolina Adamo³, Patrick Marshall³, Moheb Sheikhi¹, Tsung-Han Tsai¹, Nathan Wriedt², Clincy Cheung³, Shuoyang Qiu¹, Tien Khee Ng⁴, Qiaoqiang Gan⁴, Gambin Vincent³, Boon S. Ooi⁴, Siddharth Rajan², and Zhenqiang Ma^{1*}

¹*Department of Electrical and Computer Engineering, University of Wisconsin-Madison, Madison, Wisconsin, 53706, USA*

²*Department of Electrical and Computer Engineering, The Ohio State University, Columbus, OH 43210, USA*

³*Northrop Grumman, Redondo Beach, CA 90278, USA*

⁴*Department of Electrical and Computer Engineering, King Abdullah University of Science and Technology, Thuwal 23955-6900, Saudi Arabia*

E-mail: mazq@engr.wisc.edu, rajan.21@osu.edu, boon.ooi@kaust.edu.sa

β -Ga₂O₃, an ultrawide-bandgap semiconductor, has great potential for future power and RF electronics applications but faces challenges in bipolar device applications due to the lack of p-type dopants. In this work, we demonstrate monocrystalline AlGaAs/GaAsP/ β -Ga₂O₃ n-p-n double-heterojunctions, synthesized using semiconductor grafting technology. By transfer printing an n-AlGaAs/p-GaAsP nanomembrane to the n- β -Ga₂O₃ epitaxial substrate, we simultaneously achieved AlGaAs/GaAsP epitaxial n-p junction diode with an ideality factor of 1.29 and a rectification ratio of 2.57×10^3 at ± 2 V, and grafted GaAsP/ β -Ga₂O₃ p-n junction diode exhibiting an ideality factor of 1.36 and a rectification ratio of 4.85×10^2 at ± 2 V.

Beta-phase gallium oxide (β -Ga₂O₃) is gaining attention in the semiconductor sector due to its superior electronic properties, such as an ultrawide bandgap of 4.9 eV, a high breakdown field of 10.3 MeV, and a high electron saturation velocity of 1.1×10^7 cm/s.¹⁾⁻³⁾ These attributes, coupled with the recent advancement in the epitaxy growth technology and accessibility to large diameter native substrates, make β -Ga₂O₃ a promising candidate for next-generation high-speed, high-power electronics as well as solar-blind optoelectronics.

Despite the fast developments of unipolar β -Ga₂O₃ devices, such as Schottky diodes⁴⁾⁻⁶⁾, field-effect transistors⁷⁾⁻⁹⁾, and photodetectors¹⁰⁾⁻¹²⁾, a primary impediment for broader β -Ga₂O₃ device applications is the limited bipolar performance as a result of inefficient acceptor dopants for β -Ga₂O₃.¹³⁾⁻¹⁵⁾ In general, the candidate p-type dopants introduce deep acceptor levels in β -Ga₂O₃ bandgap, rendering them ineffective in generating free holes for conduction due to their elevated ionization energies. Various strategies have been proposed to address or circumvent this p-type inefficiency, as elaborated in multiple studies. For example, surface activated/direct wafer bonding has been employed to hetero-integrate β -Ga₂O₃ with other materials.¹⁶⁾⁻²⁰⁾ Deposition of p-type polycrystalline oxides such as NiO, Cu₂O on n-type β -Ga₂O₃ provides another perspective to create high-performance heterojunction devices.²¹⁾⁻²³⁾ In the meantime, utilizing micro-transfer printing technique, Zheng *et al* demonstrated Si/ β -Ga₂O₃ heterojunction photodetectors, which exhibited improved photoresponsivity and quantum efficiency.²⁴⁾ All these prior works have advanced the β -Ga₂O₃-based bipolar devices; however, these methods still face challenges such as imperfect surfaces, intermixing of atoms, polycrystallinity, and excess interfacial traps, which may pose new challenges in further developing β -Ga₂O₃-based bipolar devices in the future. Exploring new approaches to developing β -Ga₂O₃-based bipolar devices that can overcome some, if not all, of the challenges, is needed.

Recently, a novel method utilizing semiconductor grafting technology has been introduced to create high-quality monocrystalline Si/ β -Ga₂O₃ heterojunction p-n diodes.²⁵⁾ Semiconductor grafting allows for the creation of abrupt heterojunctions with epitaxy-like interfaces between semiconductors, irrespective of lattice structures or constants.²⁶⁾⁻²⁹⁾ Unlike the conventional wafer bonding/fusion or direct deposition/transfer printing, semiconductor grafting incorporates an ultrathin oxide (UO) interlayer between two single crystalline semiconductors. This UO layer, typically sub-nanometer thick, can be introduced extrinsically through atomic layer deposition (ALD), or intrinsically via controlled interfacial oxidation. Both approaches create a well-passivated interface, suppressing the density of states and ensuring efficient charge transport across the junction through quantum

tunneling.

In this work, we present the integration of two dissimilar semiconductor material systems, GaAs-based III-Vs (consisting of GaAs/AlGaAs/GaAsP triple layers) and β -Ga₂O₃, using semiconductor grafting technology. As a result, a double-heterojunction structure, specifically, the n-p-n AlGaAs-GaAsP- β -Ga₂O₃, was synthesized. The first heterojunction (HJ1) of n-p AlGaAs/GaAsP was formed epitaxially through conventional heteroepitaxy and was subsequently grafted to a n-type β -Ga₂O₃ epitaxial substrate. This in turn leads to a second heterojunction (HJ2) of p-n GaAsP/ β -Ga₂O₃, interfaced by a sub-nanometer thick Al₂O₃ layer. Both heterojunctions were fabricated into diodes, and current-voltage (I-V) characterizations reveal high-performance rectifying behaviors in terms of ideality factors and rectification ratios. The direct comparison between the two junctions, one formed by epitaxy and the other via grafting, suggests that the lattice-mismatched heterojunction created by semiconductor grafting can rival the quality of lattice-matched epitaxy. The advancement could facilitate the construction of more complicated device architectures, such as heterojunction bipolar transistors (HBTs), and could eventually harness the full electronic potential of β -Ga₂O₃.

The schematic of the synthesized n-p-n double-heterojunction structure is depicted in Fig. 1(a). The first epitaxial heterojunction (HJ1) consists of a 180 nm n-type Al_{0.3}Ga_{0.7}As and 80 nm p-type GaAsP. A top 100 nm heavily doped n-type GaAs layer is capped for protection of underlying AlGaAs and to facilitate effective carrier injection as the n⁺ contact layer. The second grafted heterojunction (HJ2) is formed between the 80 nm p-type GaAsP and 250 nm n-type β -Ga₂O₃, with an ultrathin interfacial Al₂O₃ for double-side passivation and quantum tunneling, which are required for grafting.²⁶⁾ Assuming a negligible potential drop at the Al₂O₃ layer, the band alignment of the n-p-n GaAs/AlGaAs/GaAsP/ β -Ga₂O₃ double heterostructure under equilibrium is illustrated in Fig. 1(b). The bandgap values adopted for GaAs, AlGaAs, GaAsP and β -Ga₂O₃ are 1.42 eV, 1.80 eV, 1.84 eV, and 4.9 eV, respectively. Their respective electron affinity values are 4.07 eV, 3.74 eV, 3.80 eV, and 4.00 eV.

The growth of the β -Ga₂O₃ n⁺⁺ sub-collector and n-type collector on an unintentionally doped (UID) β -Ga₂O₃ substrate was accomplished by plasma-assisted molecular beam epitaxy (PAMBE) using the Riber M7 system equipped with a Veeco O₂ bulb plasma source. The (010) oriented β -Ga₂O₃ UID substrate was cleaned of organics using a combination of acetone, methanol, and IPA before being loaded into the buffer of the system. The sample was baked at 400 °C for one hour to desorb any contaminants before being loaded into the main chamber for growth. The sample was heated to a substrate temperature of 725 °C before

the oxygen plasma was struck at a plasma power of 250 W and an oxygen flow of 2.5 sccm as confirmed by a mass flow controller. A Ga flux of 1.5×10^{-7} Torr as measured by nude filament gauge was used for the growth of the sub-collector. The growth rate at this condition is estimated to be ~ 4.5 nm/min from estimation of the separation between satellite peaks in an $\beta\text{-(Al}_x\text{Ga}_{1-x})_2\text{O}_3/\beta\text{-Ga}_2\text{O}_3$ superlattice structure grown at the same condition. The growth of the 100 nm thick heavily doped n++ sub-collector was accomplished by introducing several delta doped layers by using a pulsed shuttering scheme for the Si effusion cell, which was at a temperature of 1050 °C. The shutter was opened for a period of 4 seconds followed by a period of 14 seconds closed, resulting in peak Si concentrations greater than 10^{20} cm⁻³. The growth was stopped by shutting off the O₂ plasma and closing the Ga effusion cell shutter in order to move to the uniformly doped condition for the 250 nm thick n- collector. The growth was restarted with an increased plasma power of 300 W and reduced Ga flux of 1.1×10^{-7} Torr, resulting in a Si concentration of 1×10^{17} cm⁻³ as confirmed by secondary-ion mass spectroscopy (SIMS). The background Si concentration at this condition is likely coming from impurities in the quartz plasma source as has been previously reported¹.

The fabrication of the AlGaAs/GaAsP/ $\beta\text{-Ga}_2\text{O}_3$ double-heterojunction structure can be divided into two major stages, nanomembrane (NM) grafting and diode formation, as depicted in Fig. 2(a) and (b), respectively. During the initial grafting stage, the GaAs/AlGaAs/GaAsP epitaxial layers, as shown in Fig. 2(a i), was first patterned by 9×9 μm^2 mesh holes with a gap of 55 μm , using conventional photolithography. An inductively coupled plasma-reactive ion etching (ICP-RIE) process (Plasma Therm 770 ICP etcher, BCl₃: 10 sccm, and Ar: 5 sccm, pressure 15 mTorr, RIE power 60 W, and ICP power 500 W) was then employed to transfer the mesh hole pattern through the GaAs/AlGaAs/GaAsP layers, exposing the underlying sacrificial AlAs layer. The GaAs/AlGaAs/GaAsP NM was subsequently released by immersing the dry-etched epi in diluted hydrofluoric acid (HF:H₂O = 1:800) for 2 hours to chemically remove the sacrificial AlAs layer, as depicted in Fig. 1(a ii). After wet etching, the freestanding GaAs/AlGaAs/GaAsP NM, demonstrated in Fig. 1(a iii), was picked up from its source GaAs substrate using a polydimethylsiloxane (PDMS) stamp, preparing it for NM transfer printing, as illustrated in Fig. 1(a iv).

In parallel with the NM release process, contact metallization was performed on the n-/n+ $\beta\text{-Ga}_2\text{O}_3$ substrate prior to grafting, considering the potential thermal impact on the ultrathin interfacial oxide in subsequent fabrication processes. The metallization process started with dry etching of the top n- layer of the $\beta\text{-Ga}_2\text{O}_3$ substrate (Fig. 1(a I)) using the same ICP etcher (BCl₃: 18 sccm, Cl₂: 10 sccm, and Ar: 5 sccm, pressure 20 mTorr, RIE power 75 W, and ICP

power 500 W). Upon exposure of the n+ Ga₂O₃ layer, cathode metal pads were deposited using a Ti/Au/Cu/Au metal stack (10/10/100/10 nm) through an electron beam evaporator (Angstrom Engineering Nexdep Physical Vapor Deposition Platform), followed by metal lift-off process and an ohmic rapid thermal annealing (RTA) at 600 °C for 10 seconds, as schematically shown in Fig. 2(a II). After completing the metallization step, the β-Ga₂O₃ substrate was cleaned by sonication in acetone, isopropyl alcohol (IPA), and deionized (DI) water for 10 minutes each, then dipped in buffered HF (HF:H₂O = 1:10) for 1 minute. Directly after cleaning, the β-Ga₂O₃ substrate was put in a nitrogen bag and transferred into an ALD chamber, where 5 cycles of Al₂O₃ (~0.5 nm) were deposited at 250 °C. Following the ALD process, the released GaAs/AlGaAs/GaAsP NM was transfer printed to the n-region of the metallized β-Ga₂O₃ substrate with the assistance of a PDMS stamp. The grafting process was finalized with an annealing process at 350 °C for 5 minutes, allowing the formation of chemical bonding between the interfacial Al₂O₃ and the neighboring semiconductors, GaAsP and β-Ga₂O₃, resulting in the double-heterojunction structure, as schematically illustrated in Fig.2 (b i).

In the second stage of the double-heterojunction structure fabrication, another cathode metallization (Pd/Ge/Au/Cu/Au: 30/40/10/250/50 nm) was performed on the top n+ GaAs layer using the same e-beam evaporator, as shown in Fig.2 (b ii). By employing the metal on the n+ GaAs layer as an etching shadow mask, the GaAs/AlGaAs were dry etched at the exposed areas with the same ICP etcher and etching recipe, reaching the underlying p+ GaAsP layer, as displayed in Fig.2 (b iii). An anode metallization followed on the p+ GaAsP layer, using the metal stack of Ti/Pt/Au/Cu/Au: 15/50/20/300/100 nm, in the same e-beam evaporator. Afterwards, the GaAs/AlGaAs/GaAsP double heterojunction structures were isolated from each other by covering individual devices with photoresist (PR) serving as etching masks, and etched through the exposed membrane areas, as observed in Fig.2 (b v). After isolation, all the double-heterojunction devices were surface passivated with 80 cycles of Al₂O₃ (~8 nm) with the same ALD system. The final device structure is schematically demonstrated in Fig.2 (b vi).

An atomic force microscopy (AFM) image of the as-grown n-/n+ β-Ga₂O₃ substrate is presented in Fig. 3(a), displaying an ultralow surface roughness with a root mean square (RMS) value of only 0.67 nm within a scanning area of 5 × 5 μm². Fig. 3(b) presents a differential interference contrast (DIC) microscope image of the GaAs/AlGaAs/GaAsP NM transfer printed to β-Ga₂O₃ substrate upon completion of the chemical bonding process. As can be seen, the grafted NM is free of local defects such as wrinkles and air gaps, indicating

a high-fidelity micro transfer process, as well as the well-preserved NM completeness. Fig. 3(c) illustrates the DIC microscopic images of the fabricated double-heterojunction structure with the interfingered electrodes of the HJ1 in Fig. 3(c i) representing the cathode on the AlGaAs layer and the anode on the GaAsP layer. Fig. 3(c ii) depicts a cathode metal pad formed on the exposed n+ β -Ga₂O₃ layer for ohmic contact. A three-dimensional optical scan of the device is displayed in Fig. 3(d), representing a three-layered device structure, consisting of AlGaAs, GaAsP, and β -Ga₂O₃ from top to bottom.

The I-V characterizations of the double-heterojunction devices were carried out using a Keithley 4200 Parameter Analyzer. Fig. 4 shows the measured I-V relationship for the n-p AlGaAs/GaAsP (marked in red) and the p-n GaAsP/ β -Ga₂O₃ (marked in blue) heterojunctions. Both curves present comparable rectifying behaviors. The ON/OFF ratios at ± 2 V for AlGaAs/GaAsP HJ1 and GaAsP/ β -Ga₂O₃ HJ2 are 2.57×10^3 and 4.85×10^2 , respectively, while the ideality factors are calculated to be 1.29 and 1.36, respectively. The low ON/OFF ratio of both heterojunctions can currently be attributed to the absence of appropriate thermal annealing for the AlGaAs cathode and GaAsP anode, leading to early influences of the series resistance and a limited forward current level. Despite the under-optimized fabrication process, the initial I-V measurements reveal that the grafted heterojunction exhibits equivalent performance to the epitaxial heterojunction.

In summary, this work demonstrates the potential of using semiconductor grafting technology to synthesize an epitaxy-like lattice-mismatched heterojunction of GaAsP/ β -Ga₂O₃. This approach provides a viable solution to the challenge of deficient p-type doping in β -Ga₂O₃. Preliminary characterizations indicate that high-performance bipolar β -Ga₂O₃ devices for high-speed, high-power electronics, and optoelectronics can be anticipated in the future.

Acknowledgments

The work was supported by a CRG grant (2022-CRG11-5079.2) by the King Abdullah University of Science and Technology (KAUST). The work also received partial support from DARPA H2 program under grant: HR0011-21-9-0109.

References

- 1) M. Higashiwaki, K. Sasaki, H. Murakami, Y. Kumagai, A. Koukitu, A. Kuramata, T. Masui and S. Yamakoshi, *Semiconductor Science and Technology* **31** [3], 034001 (2016).

- 2) J. Y. Tsao, S. Chowdhury, M. A. Hollis, D. Jena, N. M. Johnson, K. A. Jones, R. J. Kaplar, S. Rajan, C. G. Van de Walle, E. Bellotti, C. L. Chua, R. Collazo, M. E. Coltrin, J. A. Cooper, K. R. Evans, S. Graham, T. A. Grotjohn, E. R. Heller, M. Higashiwaki, M. S. Islam, P. W. Juodawlkis, M. A. Khan, A. D. Koehler, J. H. Leach, U. K. Mishra, R. J. Nemanich, R. C. N. Pilawa-Podgurski, J. B. Shealy, Z. Sitar, M. J. Tadjer, A. F. Witulski, M. Wraback and J. A. Simmons, *Advanced Electronic Materials* **4** [1], 1600501 (2018).
- 3) M. Higashiwaki, K. Sasaki, H. Murakami, Y. Kumagai, A. Koukitu, A. Kuramata, T. Masui and S. Yamakoshi, *Semiconductor Science and Technology* **31** [3], 034001 (2016).
- 4) Y. Yao, R. Gangireddy, J. Kim, K. K. Das, R. F. Davis and L. M. Porter, *Journal of Vacuum Science & Technology B* **35** [3], 03D113 (2017).
- 5) Q. He, W. Mu, H. Dong, S. Long, Z. Jia, H. Lv, Q. Liu, M. Tang, X. Tao and M. Liu, *Applied Physics Letters* **110** [9], 093503 (2017).
- 6) S. Ahn, F. Ren, L. Yuan, S. J. Pearton and A. Kuramata, *ECS Journal of Solid State Science and Technology* **6** [1], P68 (2017).
- 7) M. Higashiwaki, K. Sasaki, A. Kuramata, T. Masui and S. Yamakoshi, *Applied Physics Letters* **100** [1], 013504 (2012).
- 8) M. Higashiwaki, K. Sasaki, T. Kamimura, M. Hoi Wong, D. Krishnamurthy, A. Kuramata, T. Masui and S. Yamakoshi, *Applied Physics Letters* **103** [12], 123511 (2013).
- 9) W. S. Hwang, A. Verma, H. Peelaers, V. Protasenko, S. Rouvimov, H. (Grace) Xing, A. Seabaugh, W. Haensch, C. V. de Walle, Z. Galazka, M. Albrecht, R. Fornari and D. Jena, *Applied Physics Letters* **104** [20], 203111 (2014).
- 10) T. Oshima, T. Okuno, N. Arai, N. Suzuki, S. Ohira and S. Fujita, *Applied Physics Express* **1** [1], 011202 (2008).
- 11) W.-Y. Kong, G.-A. Wu, K.-Y. Wang, T.-F. Zhang, Y.-F. Zou, D.-D. Wang and L.-B. Luo, *Advanced Materials* **28** [48], 10725 (2016).
- 12) X. Chen, K. Liu, Z. Zhang, C. Wang, B. Li, H. Zhao, D. Zhao and D. Shen, *ACS Appl. Mater. Interfaces* **8** [6], 4185 (2016).
- 13) A. Kyrtos, M. Matsubara and E. Bellotti, *Applied Physics Letters* **112** [3], 032108 (2018).
- 14) S. J. Pearton, J. Yang, P. H. Cary IV, F. Ren, J. Kim, M. J. Tadjer and M. A. Mastro, *Applied Physics Reviews* **5** [1], 011301 (2018).
- 15) Y. Su, D. Guo, J. Ye, H. Zhao, Z. Wang, S. Wang, P. Li and W. Tang, *Journal of Alloys and Compounds* **782**, 299 (2019).
- 16) Z. Cheng, F. Mu, T. You, W. Xu, J. Shi, M. E. Liao, Y. Wang, K. Huynh, T. Suga, M. S. Goorsky, X. Ou and S. Graham, *ACS Appl. Mater. Interfaces* **12** [40], 44943 (2020).
- 17) C.-H. Lin, N. Hatta, K. Konishi, S. Watanabe, A. Kuramata, K. Yagi and M. Higashiwaki, *Applied Physics Letters* **114** [3], 032103 (2019).
- 18) T. Matsumae, Y. Kurashima, H. Umezawa, K. Tanaka, T. Ito, H. Watanabe and H. Takagi, *Applied Physics Letters* **116** [14], 141602 (2020).
- 19) P. Sittimart, S. Ohmagari, T. Matsumae, H. Umezawa and T. Yoshitake, *AIP Advances* **11** [10], 105114 (2021).
- 20) Y. Xu, F. Mu, Y. Wang, D. Chen, X. Ou and T. Suga, *Ceramics International* **45** [5], 6552 (2019).
- 21) W. Hao, Q. He, X. Zhou, X. Zhao, G. Xu, and S. Long, in *2022 IEEE 34th International Symposium on Power Semiconductor Devices and ICs (ISPSD)* (2022) pp. 105.
- 22) J. Zhang, P. Dong, K. Dang, Y. Zhang, Q. Yan, H. Xiang, J. Su, Z. Liu, M. Si, J. Gao, M. Kong, H. Zhou and Y. Hao, *Nature Communications* **13** [1], 3900 (2022).

- 23) P. Schlupp, D. Splith, H. von Wenckstern and M. Grundmann, *physica status solidi (a)* **216** [7], 1800729 (2019).
- 24) Y. Zheng, M. N. Hasan and J.-H. Seo, *Advanced Materials Technologies* **6** [6], 2100254 (2021).
- 25) J. Gong, D. Kim, H. Jang, F. Alema, Q. Wang, T. Khee Ng, S. Qiu, J. Zhou, X. Su, Q. Lin, R. Singh, H. Abbasi, K. Chabak, G. Jessen, C. Cheung, V. Gambin, S. S. Pasayat, A. Osinsky, Boon, S. Ooi, C. Gupta and Z. Ma, *arXiv e-prints arXiv:2305.19138* (2023).
- 26) D. Liu, S. J. Cho, J.-H. Seo, K. Kim, M. Kim, J. Shi, X. Yin, W. Choi, C. Zhang, J. Kim, M. A. Baboli, J. Park, J. Bong, I.-K. Lee, J. Gong, S. Mikael, J. H. Ryu, P. K. Mohseni, X. Li, S. Gong, X. Wang and Z. Ma, *arXiv e-prints arXiv:1812.10225* (2018).
- 27) D. Liu, S. J. Cho, J. Park, J. Gong, J.-H. Seo, R. Dalmau, D. Zhao, K. Kim, M. Kim, A. R. K. Kalapala, J. D. Albrecht, W. Zhou, B. Moody and Z. Ma, *Applied Physics Letters* **113** [1], 011111 (2018).
- 28) D. Liu, S. J. Cho, J. Park, J.-H. Seo, R. Dalmau, D. Zhao, K. Kim, J. Gong, M. Kim, I.-K. Lee, J. D. Albrecht, W. Zhou, B. Moody and Z. Ma, *Applied Physics Letters* **112** [8], 081101 (2018).
- 29) S. J. Cho, D. Liu, A. Hardy, J. Kim, J. Gong, C. J. Herrera-Rodriguez, E. Swinnich, X. Konstantinou, G.-Y. Oh, D. G. Kim, J. C. Shin, J. Papapolymerou, M. Becker, J.-H. Seo, J. D. Albrecht, T. A. Grotjohn and Z. Ma, *AIP Advances* **10** [12], 125226 (2020).

Figure Captions

Fig. 1. (a) Schematic illustration of the GaAs/AlGaAs/GaAsP/ β -Ga₂O₃ n-p-n double-heterojunction (HJ) structure, with the epitaxial HJ1 comprising AlGaAs and GaAsP, and the grafted HJ2 formed between GaAsP and β -Ga₂O₃. (b) Band alignment of the GaAs/AlGaAs/GaAsP/ β -Ga₂O₃ heterostructure at equilibrium.

Fig. 2. Process flow illustration of the GaAs/AlGaAs/GaAsP/ β -Ga₂O₃ n-p-n double-heterojunction. (a) The grafting process, where GaAs/AlGaAs/GaAsP membrane is released from its source substrate and then transfer printed to the β -Ga₂O₃ substrate, which is pre-patterned with cathode pads and surface coated with Al₂O₃. (b) Device fabrication of the with a double mesa formation and triple metal deposition on respective layers. Each layer is

represented by different colors, with their detailed materials indexed at the bottom of the figure.

Fig. 3. (a) An atomic force microscope (AFM) scanning of the as-grown β -Ga₂O₃ substrate. (b) Differential interference contrast (DIC) microscopic image of the GaAs/AlGaAs/GaAsP nanomembrane transferred on β -Ga₂O₃ substrate. (c) DIC microscopic images of fabricated devices, with i) interfingered cathode on GaAs/AlGaAs and anode on GaAsP, and ii) a cathode metal pad formed on n+ β -Ga₂O₃. (d) Three-dimensional optical profiling of the fabricated heterostructure.

Fig. 4. Measured I-V characteristics of the AlGaAs/GaAsP HJ1 and the GaAsP/ β -Ga₂O₃ HJ2, presented on (a) the linear scale, and (b) the semi-logarithmic scale. The inset of (a) indicates the respective locations of HJ1 and HJ2, while the inset of (b) summarizes the extracted ON/OFF ratios and ideality factors from the measured curves.

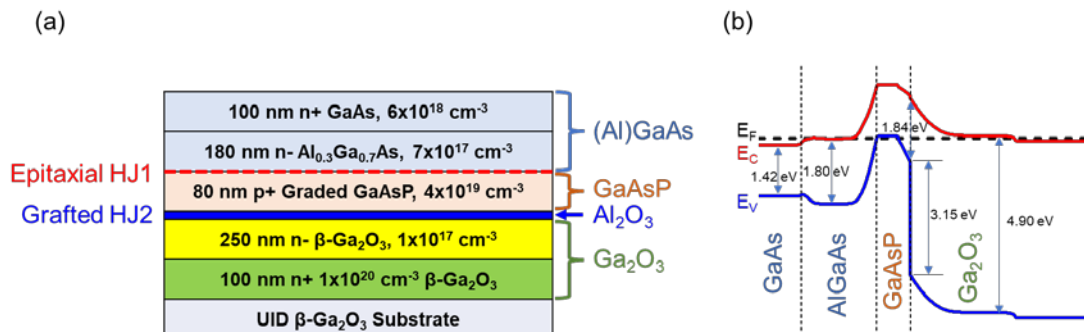


Fig.1.

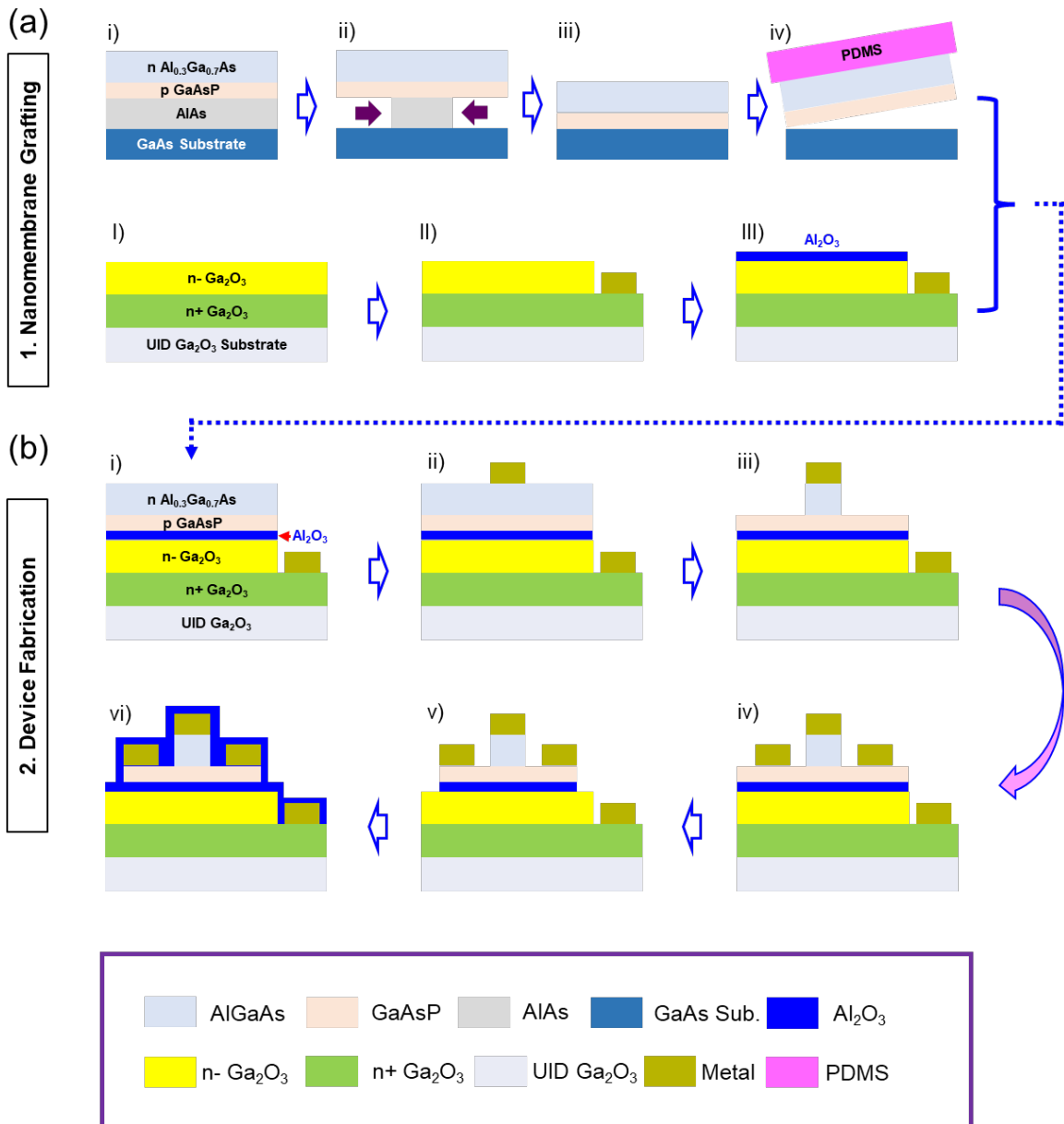


Fig. 2.

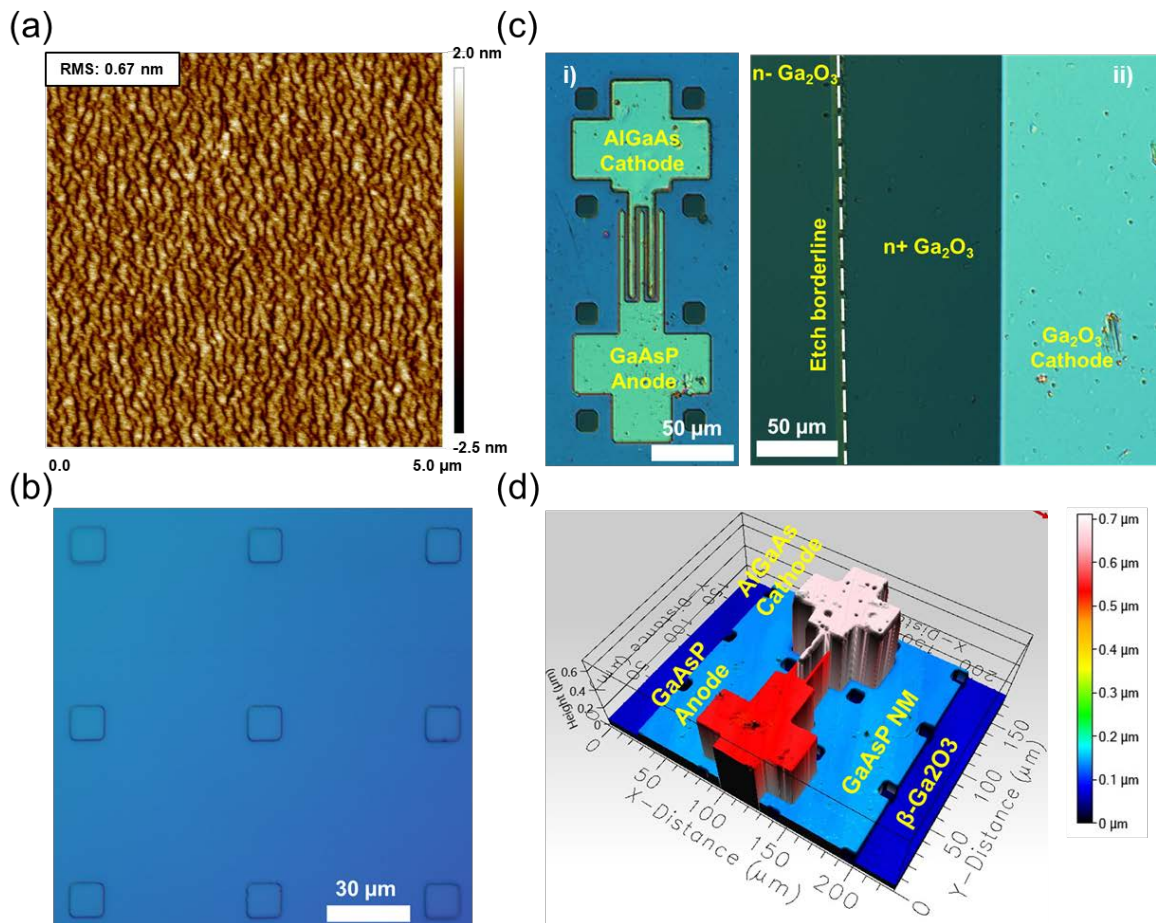


Fig. 3.

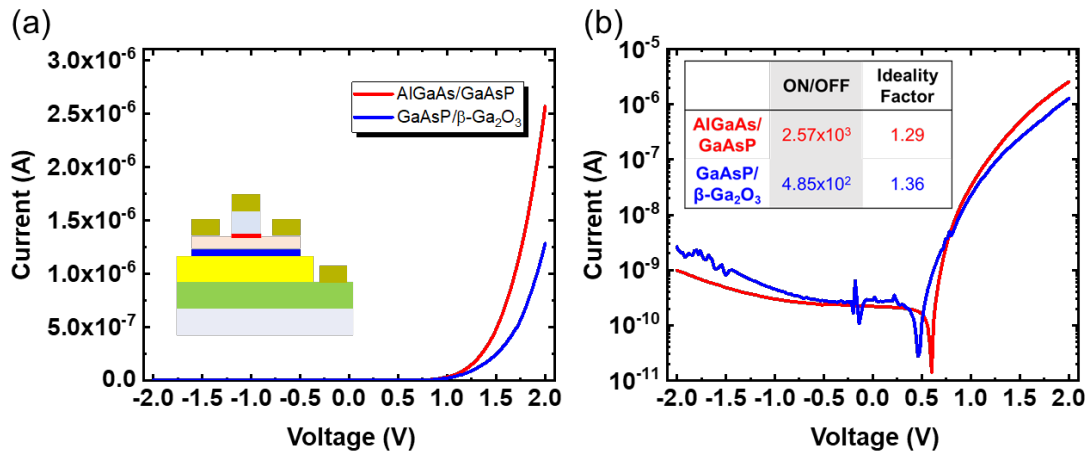


Fig. 4.